Results in Engineering 17 (2023) 100793

Contents lists available at ScienceDirect

Results in Engineering

journal homepage: www.sciencedirect.com/journal/results-in-engineering

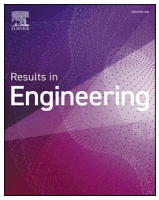

Micro-embossing of micro-structures in RSA-501 as mold inserts for the replication of micro-lens arrays

Julian Kober [a,*], Daniel Rolón [a], Florian Hölzel [b], Stefan Kühne [a], Dirk Oberschmidt [a], Thomas Arnold [b]

[a] Berlin Institute of Technology, Institute of Machine Tools and Factory Management, Micro and Precision Devices, Pascalstr. 8–9, 10587, Berlin, Germany
[b] Leibniz Institute of Surface Engineering (IOM), Permoserstr. 15, 04318, Leipzig, Germany

ARTICLE INFO

Keywords:
Rapidly solidified aluminum
RSA-501
Micro-embossing
Nanoindentation
Micro-lens arrays

ABSTRACT

The production of mold inserts for the replication of micro-lens arrays through micro-embossing could be an alternative process route compared to diamond turning or milling in order to reduce time and costs. The rapidly solidified aluminum alloy RSA-501 is expected to form micro-structures with low surface roughness because of its ultra-fine grain structure. In micro-embossing challenges like elastic spring back effect, pile-ups, and forming accuracy depend on the material behavior. Therefore, RSA-501 was further characterized and the influence of polishing or flycutting on the material behavior was investigated. To further understand the grain and micro-structure samples were sectioned along their cross and longitudinal directions. The grain structure of RSA-501 was oriented along the extrusion direction and the mean grain sizes were <1.00 μm. Furthermore, RSA-501 was micro-embossed to investigate the influence of the material behavior and surface preparation on the forming of micro-structures. The induced surface integrity through flycutting was not deep enough to influence the forming of micro-structures. Therefore, the workpiece surface can be prepared either by polishing or flycutting. When micro-embossing RSA-501, cross and longitudinal sections can be used. However, it is recommended to process the cross section because of its isotropic grain structure. It was shown that the curvature radius of micro-embossed concave structures differs from the tool radius. This is due to the elastic spring back effect. Since the embossed structure remains spherical, the spring back effect can be compensated by adjusting the tool radius.

1. Introduction

Micro-lens arrays (MLA) are micro-optical components that consist of a large number of lenslets. In comparison to single aperture optics MLAs have the benefit of combining a large field of view with a small optical component volume [1]. Additionally, MLAs have a low aberration and distortion, high temporal resolution, and infinite depth of field [2]. However, MLAs have a low resolution and sensitivity [3]. Under the condition that high-resolution is not always required, MLAs can provide a miniaturization of optical systems [1]. Applications of MLAs are mostly common in light field cameras [4], sensors, beam homogenization of lasers and other photonic devices [5].

A review on the range of manufacturing methods to produce MLAs is given, e. g. by Yuan et al. [2] and Cai et al. [6], see Fig. 1. The production of MLAs via the direct route does not rely on a mold insert or mask. These methods are simple but the micro-lens geometry has to be controlled by the process parameters such as temperature, wettability, pressure, and process time. Indirect methods control the micro-lens geometry by using a mold insert but are more complex [2]. Replication is then carried out in polymers or glass [7].

Cost-efficient production of MLAs relies on the replication process of a master structure. Therefore, mold inserts that have a negative form of the structure to be replicated are manufactured. Ultra-precision machining processes such as milling and single point diamond turning

Abbreviations: MLA, Micro-lens array; SPDT, Single point diamond turning; RSA, Rapidly solidified aluminum; CS, cross section; LS, longitudinal section; RSP, Rapid solidification processing; EBSD, Electron backscatter diffraction; SEM, Scanning electron microscope; FIB, Focused ion beam; AFM, Atomic force microscope; WLI, White light interferometer; LSM, Laser scanning microscope; EDX, Energy dispersive X-ray spectroscopy; BSE detector, Back-scattered electron detector; PSD, Power spectral density functions.

* Corresponding author.
E-mail address: kober@mfg.tu-berlin.de (J. Kober).

https://doi.org/10.1016/j.rineng.2022.100793
Received 18 August 2022; Received in revised form 14 November 2022; Accepted 22 November 2022
Available online 1 December 2022

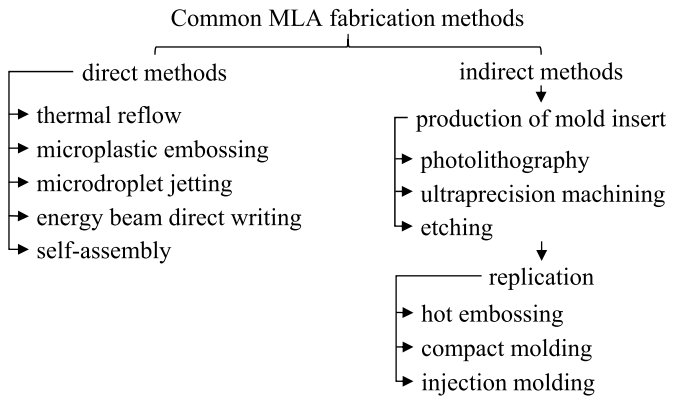

Fig. 1. Common MLA fabrication methods, according to [2,6].

(SPDT) with fast-tool-servo or slow-slide-servo have been extensively investigated in order to produce mold inserts [8].

However, SPDT requires expensive ultra-precision machine-tools, single-crystal diamond tools, and set-up time. The here proposed micro-embossing of mold inserts could be an alternative in order to manufacture MLAs cost-efficient. This method consists of two steps. At first, the workpiece surface needs to be prepared either by polishing or machining. The reason is that the surface of the specimen has to be plane-parallel with regard to the table surface and of low surface roughness Sq $<$ 10 nm in order to be micro-embossed. Defects such as scratches, pores, and machining marks in the surface will be present in embossed micro-structures as well. Therefore, samples need to be prepared either by polishing or machining according to these specifications. Secondly, the structures are micro-embossed using ruby tools. Advantages of this method are reduced set-up time, process time, and tool costs, since the embossing tools made of ruby are cheaper than diamond tools and the machinery is simpler and easier to handle than ultra-precision machine-tools [9].

Micro-embossing as carried out here is a manufacturing technology within the group compression forming. This group contains the technologies rolling, free forming, die forming, embossing, and extrusion [10]. The forming technology micro-forging is closely related is to micro-embossing. The advantages of micro-embossing in comparison to micro-forging are that the process does not need elevated temperature and preparation of spherical cavities beforehand [11]. Therefore, a lot of process time for cavities preparation, heating, pressure holding, and cooling can be saved. A single embossing only takes a few seconds. Thus, it is possible to use a single ball as tool for forming a huge amount of embossings and arrange these as wished as long as the pile-ups can be controlled. The arrangement of embossings does not rely on an arrangement of ball-shaped tools. This makes new arrangements possible. In addition, using a single ball-shaped tool does not have the disadvantage of variating ball diameters.

Rapidly solidified aluminum (RSA) alloys are mostly employed in ultra-precision machining of optical elements alongside with conventional aluminum alloys. Due to their ultra-fine grains RSA-alloys enable a very low surface roughness when compared to conventional aluminum alloys [12]. Within this context, the ultra-fine grains of RSA alloys are the basis for machining samples with low surface roughness, because the smaller the grains and the more evenly they are distributed, the lower the surface roughness that can be achieved. The reason for the ultra-fine grain of RSA is the rapid solidification processing (RSP). The main step of RSP is the melt spinning process, which allows extremely high cooling rates of up to 10^6 K/s (a). To reach such high cooling rates the alloyed melt is poured on a water-cooled spinning copper wheel. Ribbons are formed and are protected from oxidation by inert gas [13]. The ribbons are chopped into fine flakes and consolidated into billets. Those billets can then be processed by hot extrusion at temperatures 300 °C–380 °C. If the alloy can be aged, a heat treatment can be applied during or after the hot extrusion to allow the formation of precipitations [14].

RSA-501 is an ultra-fine grained material, which allows to form micro-structures with low surface roughness. However, RSA-501 is yet not fully characterized as researches were mainly focused on its precipitations and strength [14]. RSA-501 is composed of AlMg5Mn1Sc0.8Zr0.4 and is made by RSP Technology, Netherlands. Due to the exceptionally high cooling rates the homogeneous melt is being frozen, which creates a supersaturated Al-solid. The Sc and Zr fractions dissolved in the Al-solid are higher than their maximal solubility of 0.38 wt% Sc and 0.28 wt% Zr [15] at eutectic temperature. Sc increases the strength of RSA-501 by grain refinement due to increased nucleation during solidification and by precipitation hardening. During the ageing of RSA-501 nano-sized spherical Al_3Sc, Al_3Zr and most importantly $Al_3Sc_xZr_{1-x}$ precipitations are formed. Because of the slow diffusivity of Zr in the Al-solid the $Al_3Sc_xZr_{1-x}$ precipitations have an Al_3Sc core and an Al_3Zr shell [16]. When aging RSA-501 at 300 °C for 8 h, Palm et al. observed that $Al_3Sc_xZr_{1-x}$ precipitations have a size of 2 nm–4 nm. They increase the strength for each fraction of 0.1 wt% Sc by approx. 45 MPa [14]. Additionally, Al_6Mn phases are formed at sub-grain boundaries, but do not affect the hardness of RSA-501 [17].

Until now RSA-501 is not often used for micro-forming processes. In micro-forming and micro-embossing structures in the single micrometer range are formed through plastic deformation [18]. In that range the friction between tool and workpiece, the material's microstructure and the spring back effect become a challenge [19]. Another challenge is anisotropic material behavior if a dimension of a feature is comparable to the material's grain size [20]. To achieve quasi-isotropic material behavior Justinger [21] recommends to have at least 50 grains in the cross section of a feature. Hence, using an ultra-fine grained material avoids anisotropic material behavior in micro-forming [20].

Since the micro-structures of mold inserts are manufactured through micro-forming, the material properties directly influence the geometry of embossed micro-structures. Therefore, this paper aims at investigating how the surface preparation method, RSA-501's grain structure, texture, and elastic spring back effect affect the geometry of embossed micro-structures of mold inserts.

2. Experimental set-up and method

To understand the texture and grain structures of RSA-501, cross and longitudinal sections according to the extrusion direction were segmented using wire electro-machining in a Robofil 240 by Charmilles Technologies, Switzerland. These samples were metallographically prepared by means of grinding, polishing and etching with NaOH to contrast the microstructure.

Electron backscatter diffraction (EBSD) measurements taken in a scanning electron microscope (SEM) DSM 982 GEMINI by Carl Zeiss AG, Germany, and with the Hikari XP detector by EDAX AMETEK, Inc., USA, were used to perform measurements of the specimens to investigate the material's grain structure and texture. EDX mappings were taken in a TEM Tecnai G^2 20 S-TWIN by FEI Technologies Inc., USA, and with the EDX r-TEM SUTW detector by EDAX AMETEK, Inc., USA, to examine the precipitation's elements.

In order to measure the influence of the surface preparation on the material's properties, nanoindentation investigations were performed with the Nanoindenter TI 980 by Hysitron Inc., USA, during which the reduced E-Modulus and hardness were measured.

Also, to analyze the surface integrity caused by previous processes, polished and flycut samples were prepared by using a focused ion beam (FIB) (see Fig. 2) and measured by means of SEM in the dual beam device HELIOS nanolab 600 by FEI Technologies Inc., USA.

Micro-embossing tests were conducted to investigate the influence of the material's elastic spring back effect on the geometry of micro-structures. Therefore, a self-made device was employed (see Fig. 3). The machine consists of a fast-tool-servo, a three-linear-axis system driven by stepper motors, a force measurement system and a constant

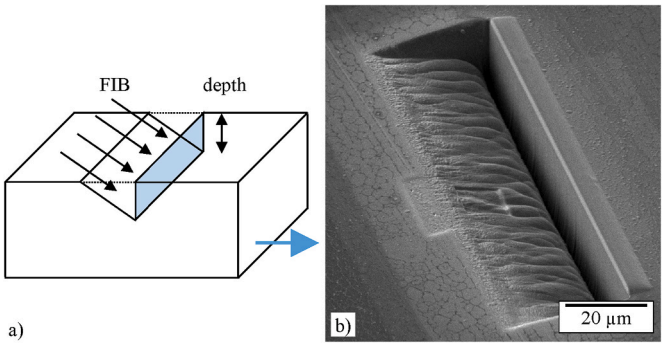

Fig. 2. a) Scheme of the focused ion beam (FIB) preparation and b) example of a wedge prepared by means of FIB for a surface integrity measurement.

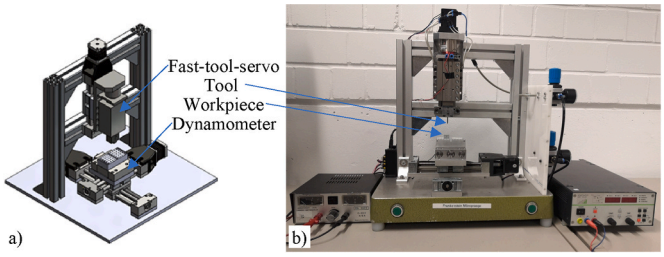

Fig. 3. a) Model and b) picture of the developed micro-embossing device.

current power supply. The fast-tool-servo from the company LT Ultra-Precision Technology GmbH, Germany, consists of a voice coil actuator, a forcer, and an air bearing. The RSA-501 specimens were fixed on the force measurement system and the tools were fixed on the forcer of the fast-tool-servo. Beforehand, the tools were made by joining ruby spheres on the tool shafts (X8CrNiS18-9) with a photopolymer (OrmoComp) as bonding agent. Tools with diameters R_r of 0.15 mm, 0.25 mm, 0.5 mm, 0.75 mm and 1.00 mm were employed.

After fixing the workpiece and the tool, micro-embossing of single concave micro-structures in RSA-501 was carried out at ambient temperature according to the simplified principle of micro-embossing in Fig. 4.

In the first step a) the embossing force was adjusted by controlling the current of the voice coil actuator through the constant current power supply. The applied embossing force is a resultant of the induced Lorentz force and the weight force, which in this case was the sum of the forcer and tool masses.

In the second step b) the workpiece surface was brought in contact with the tool. This was done by lowering the z-axis, on which the fast-tool-servo is fixed, towards the workpiece until reaching contact with the surface. The force measurement system allowed to trigger the stop of the z-axis movement, when a force difference $\Delta F = 5$ mN due to contact

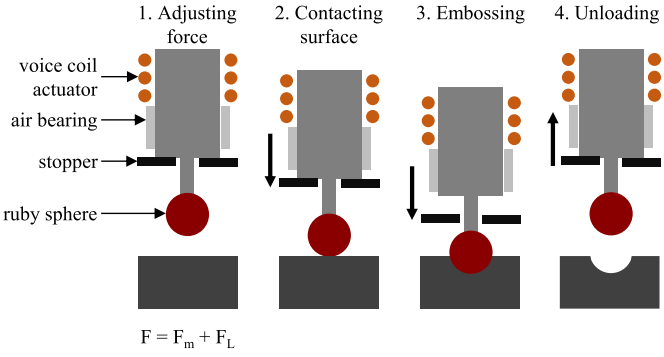

Fig. 4. Schematic principle of micro-embossing.

was measured over a period of 20 ms. The employed force measurement system was the Typ 9119AA1 by Kistler Group, Switzerland, which has a measuring threshold of <2 mN and can measure forces up to 4 kN.

In the third step c) the workpiece was embossed by lowering the z-axis by 450 µm so that the tool was lifted from the end stop, that carried the load beforehand. The embossing force was applied on the workpiece for a certain amount of time before the tool was retracted by moving up the z-axis as the fourth step d).

The effects of different parameters on the geometry of the embossed micro-structures of the mold insert were investigated by measuring the diameter d_e, depth d, pile-up height h and pile-up width w. The geometry of an embossed structure can be seen in Fig. 5a. The embossed micro-structures were measured with an atomic force microscope (AFM) NaniteAFM by Nanosurf AG, Switzerland, a white light interferometer (WLI) NPFlex by Bruker Corporation, USA, and a laser scanning microscope (LSM) VK-X3000 by Keyence Corporation, Japan. The software Gwyddion was utilized for analyzing the measurements.

3. Material characterization of RSA-501

When embossing micro-structures through metal forming, the material has a huge impact on the formation of micro-structures through inhomogeneities, plasticity, and the elastic spring back effect. Therefore, the material characterization of RSA-501 was carried out in order to investigate if a texture, inhomogeneities or defects were present.

3.1. Metallography

Metallographic examinations were carried out to investigate the material's structure, precipitations, homogeneity and texture. From the cross- (CS) and longitudinal-sectional (LS) micrographs in Fig. 6 can be seen, that RSA-501 shows a texture. Due to the rapid solidification processing the structure of compressed flakes is visible even after the hot extrusion. The flakes vary in form and size. In contrast to the cross section the flakes are elongated in the longitudinal section as a result of the hot extrusion. The compressed flakes of a Scalmalloy after hot isostatic pressing can be seen in the work of Palm et al. [14]. The visible fine precipitations in the micrographs have a size of <1 µm and appear to be round in shape.

3.2. EBSD and EDX measurements

EBSD (Electron Backscatter Diffraction) and EDX (Energy dispersive X-ray spectroscopy) measurements were carried out to investigate the material's microstructure, texture, and precipitations. The SEM micrograph in Fig. 7 taken with a back-scattered electron detector (BSE detector) shows the precipitations in RSA-501 at high magnification. Besides the grain structure mostly bright precipitations could be observed from the SEM micrograph. These precipitations were mostly located on grain boundaries.

Results of the EDX mapping can be seen in Fig. 8 a) – d). Mg is homogeneously distributed in the matrix and forms precipitations that have not been reported in literature before. The bright precipitations in Fig. 7 are rich in Mn and hence are likely to be the Al_6Mn precipitations described in literature [17]. They have a size between 50 nm and 250 nm and are likely located on the grain boundaries. Sc and Zr are homogeneously distributed in the matrix, since their precipitations are nano-sized.

The EBSD measurements in Fig. 9 indicate anisotropic texture. Grains in the cross section are round, while in the longitudinal section they are elongated. The grain size distribution of RSA-501 in Fig. 10 shows that the majority of grains are <500 nm, but a minority of grains >2 µm does exist. The mean grain size was calculated as < 1 µm, which is in accordance to the manufacture's declaration. However, the EBSD measurements show an inhomogeneous distribution of grains. Regions of ultra-fine grains and region of larger grains could be distinguished in

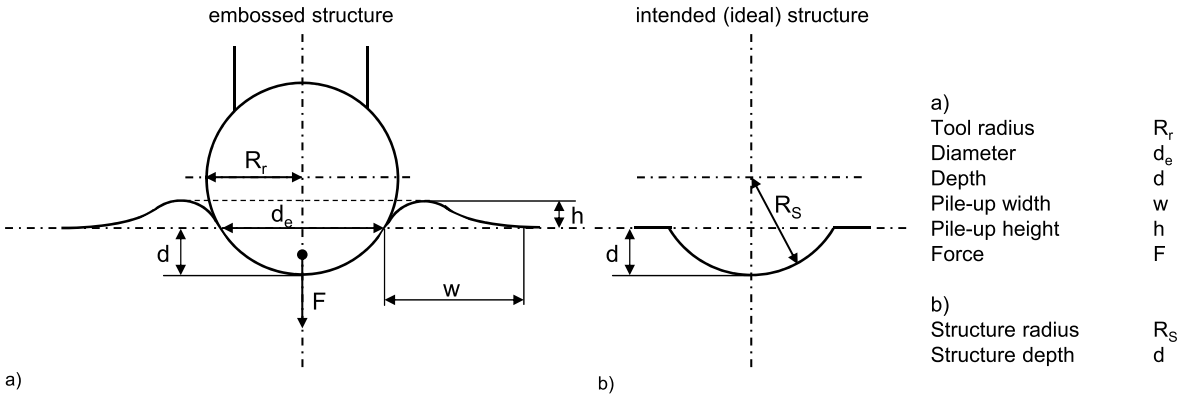

Fig. 5. Geometric parameters of a) embossed structure and b) ideal structure.

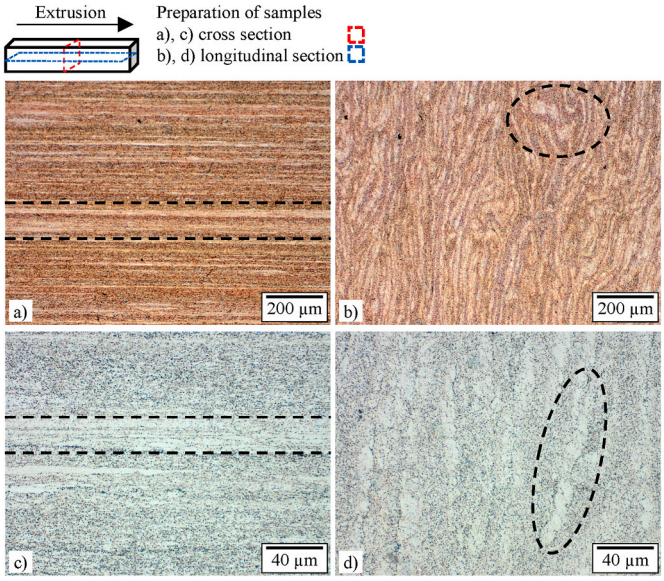

Fig. 6. Micrographs of cross and longitudinal sections of RSA-501 etched with NaOH.

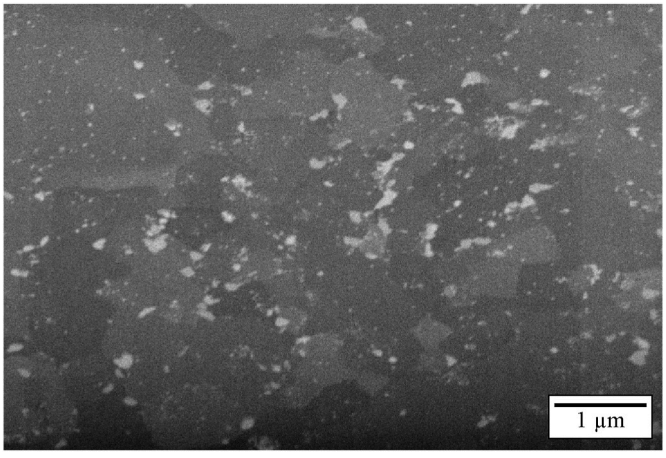

Fig. 7. SEM micrograph of RSA-501 cross-section prepared by means of FIB taken with BSE detector.

both sections.

3.3. Nanoindentation

Nanoindentation of RSA-501 was performed to investigate the influence of surface preparation and specimen orientation on the material's properties. Nanoindentation experiments were conducted on the specimens using a Berkovich indenter. A load P = 10 mN was applied to the specimens and was held for a holding time t_h = 1 s. Loading and unloading times were either t_P = 5 s or t_P = 10 s. 50 repetitions were performed for each parameter set.

In general, the load-indentation graphs (P-h-graphs) of the indentation in RSA-501 showed whether pop-in nor phase transformation as expected (see Fig. 11), but pile-ups were observed around the indents. Material properties such as E-modulus E and hardness H were calculated based on the Oliver-Pharr-method [22].

The reduced E-Modulus of the polished cross-sectional specimen E_r = 70.0 GPa was in accordance with the declaration of the manufacturer E = 70 GPa [23]. Loading and unloading times were 5 s. The cross-sectional specimen prepared by flycutting showed a higher reduced E-Modulus E_r = 110.8 GPa, see Table 1. There was no significant difference between the reduced E-Modulus E_r of longitudinal and that of the cross sections noticed, whereas the flycut longitudinal specimen had a reduced E-Modulus E_r = 112.9 GPa. When the loading times were changed to t_p = 10 s, the reduced E-Modulus E_r increased very slightly from E_r = 110.8 GPa to E_r = 113.4 GPa. The maximum indentation depth h_{max} differed between the polished and flycut specimens, but the final indentation depth h_f was nearly the same in all experiments. The hardness of the polished specimen was slightly lower (see Table 1) compared to the flycut ones, but all specimens had a nearly equal hardness value of approx. 3.0 GPa.

3.4. Surface integrity measurement

The workpiece surface preparation can cause a surface integrity due to the induced process forces and temperatures [24]. Therefore, the effect of the surface preparation on the material was investigated. The depth of the surface integrity of sections prepared by FIB was measured in a SEM to investigate the effect of the surface preparation on the surface integrity of the samples.

Specimens were either prepared by grinding and polishing or by flycutting using a monocrystalline diamond tool on a modified ultra-precision machine tool MMC1100 by LT Ultra-Precision Technology GmbH, Germany. Flycutting was employed using a tool with rake angle γ = 0°, depth of cut a_p = 5 µm, velocity of cut v_c = 942 m/min and feed rate v_f = 120 mm/min. SEM-micrographs of flycut and polished specimens can be seen in Fig. 12. The surface integrity of the samples was analyzed over a length of 50 µm because the surface integrity varies in depth along the specimen surface. The depth of the surface integrity of

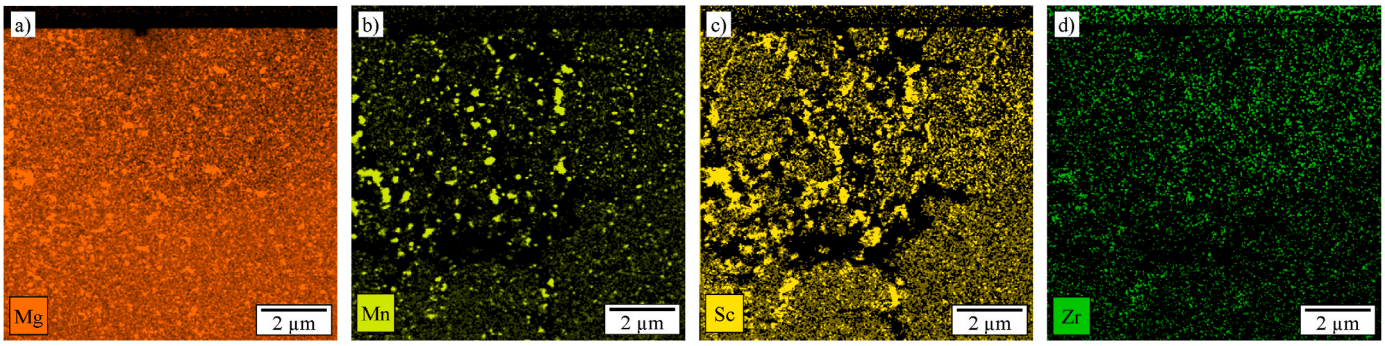

Fig. 8. EDX maps for a) Mg, b) Mn, c) Sc and d) Zr or RSA-501 (AlMg5Mn1Sc0.8Zr0.4) of the same spot.

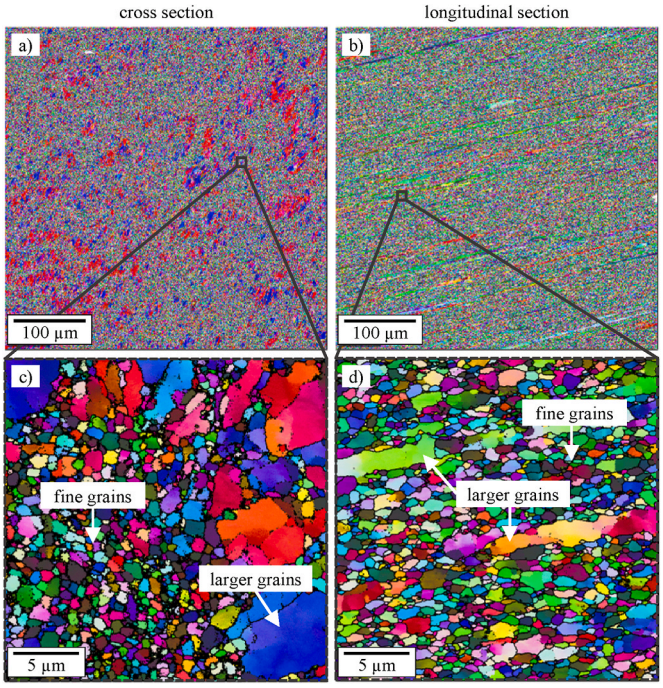

Fig. 9. EBSD mapping of a), c) cross and b), d) longitudinal section of RSA-501. Regions of fine sized grains (top) and regions of larger grains (bottom) were noticed.

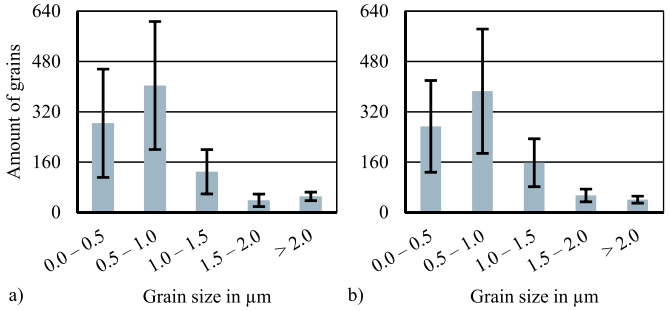

Fig. 10. Grain size distribution of a) cross section, b) longitudinal section of RSA-501. A filter is set at 0,30 µm. The mean grain sizes (caliper method) are a) d = 0.82 µm ± 0.18 µm and b) d = 0.90 µm ± 0.13 µm.

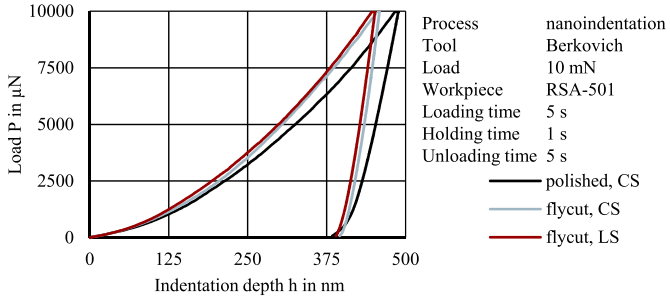

Fig. 11. P-h-graphs of nanoindentations with Berkovich indenter in cross-sectional RSA-501 specimens prepared by flycutting or polishing. Loading and unloading times were 5 s and holding time was 1 s.

Table 1
Results of nanoindentation in RSA-501.

Material	RSA-501	RSA-501	RSA-501	RSA-501
Section	longitudinal	cross	cross	cross
Preparation	flycut	polished	flycut	flycut
t_P [s]	5	5	5	10
t_h [s]	1	1	1	1
P [mN]	10	10	10	10
h_{max} [nm]	449.9 ± 6.5	487.3 ± 11.1	459.8 ± 8.1	462.8 ± 7.9
h_f [nm]	389.0 ± 6.9	399.3 ± 11.7	399.6 ± 8.8	401.0 ± 9.3
E_r [GPa]	112.9 ± 1.4	70.0 ± 1.6	110.8 ± 2.9	113.4 ± 3.6
H [GPa]	3.09 ± 0.09	2.85 ± 0.13	2.96 ± 0.11	2.91 ± 0.10

the flycut specimen was 34 nm ≤ s ≤ 192 nm, while for the polished specimen no surface integrity could be observed.

4. Micro-embossing of concave micro-structures in RSA-501

Following the characterization of RSA-501, the same specimens were used for the micro-embossing of concave micro-structures (see Fig. 13) to investigate how he formation of micro-structures in RSA-501 was affected by the surface preparation method, the texture and elastic spring back effect of the material.

Tests have shown that the holding time and embossing velocity have no effect on the geometry of micro-structures [9]. Therefore, the embossing velocity was set to v = 30 mm/min and holding time was neglected. A polished RSA-501 cross-sectional specimen was embossed with tools of different radius R_r and under variation of the embossing force F (see Table 2).

The effects of the tool radius R_r and the embossing force F can be seen in Fig. 14. The depth d decreases with an increasing tool radius R_r as expected. At the same time for forces F ≥ 5 N the diameter d_e decreases with decreasing tool radius R_r. Pile-ups are higher and wider in their form if tools of smaller radius R_r are used.

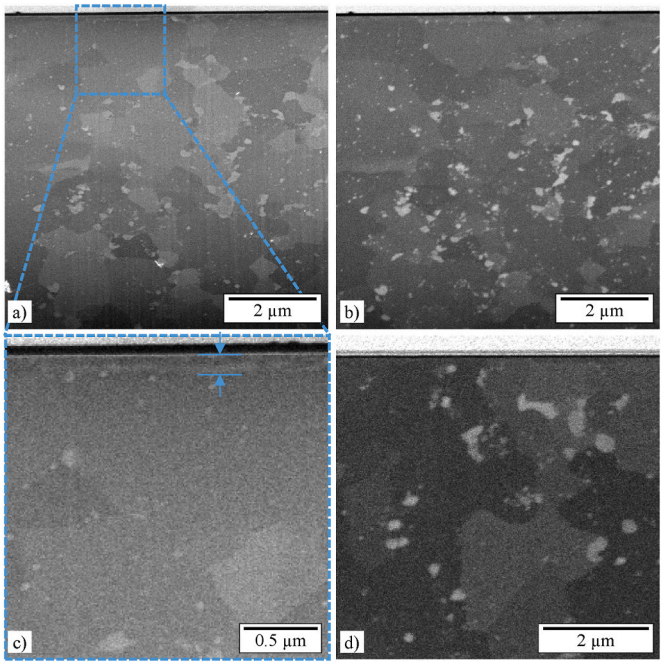

Fig. 12. SEM micrographs of sections prepared by FIB. Imaging of surface integrity of flycut cross-sectional RSA-501 specimen taken with a) the SE detector and b) the BSE detector. Micrograph a) is magnified in c). Micrograph d) shows a polished cross-sectional RSA-501 specimen taken with the BSE detector.

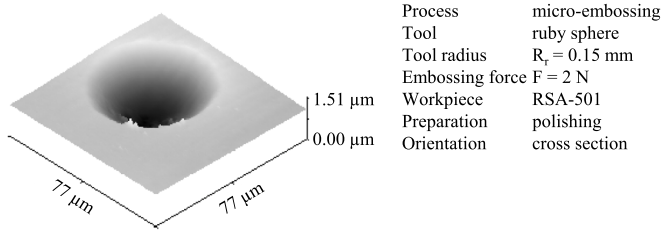

Fig. 13. AFM measurement of a micro-embossment.

Table 2
Variation of tool radius and embossing force.

Tool radius R_r [mm]	0.15	0.25	0.50	0.75	1.00
Embossing force F [N]	4	6	8		

To investigate the influence of the surface preparation on the resulting geometry, micro-structures were embossed in polished and flycut RSA-501 cross-sectional specimens and the geometry of the embossed micro-structures was measured.

Fig. 15 shows the diameter and the depth of the embossed micro-structures in dependence on the embossing force. When comparing the specimens with different surface preparations, the depths d, and diameters d_e of the embossed micro-structures in polished and flycut RSA-501 correspond well to each other. For instance, embossing with F = 6 N resulted in depths d_{pol} = 3.835 µm ± 0.272 µm and $d_{fly,CS}$ = 3.500 µm ± 0.133 µm and in diameters $d_{e,pol}$ = 72.1 µm ± 1.9 µm and $d_{e,fly,CS}$ = 72.0 µm ± 0.9 µm.

An additional flycut longitudinal-sectional specimen was embossed to investigate the effect of the texture of RSA-501 on micro-embossed structures. The depth and diameter of the micro-structures in flycut longitudinal and cross-sectional specimens showed no significant difference. For instance, embossing with F = 6 N resulted in depths $d_{fly,CS}$ = 3.500 µm ± 0.133 N and $d_{fly,LS}$ = 3.810 µm ± 0.212 µm and in diameters $d_{e,fly,CS}$ = 72.0 µm ± 0.9 µm and $d_{e,fly,LS}$ = 72.5 µm ± 1.5 µm.

The results of the pile-up height h and pile-up width w can be seen in Fig. 15. It has to be pointed out that the pile-up values are maximum values. The pile-ups varied strongly between micro-structures since pile-ups were randomly organized around the indents. The pile-ups height h and width w were found to increase with increasing embossing force F.

LSM measurements of the prepared surfaces, embossed micro-structures and a replicated structure were analyzed to calculate the power spectral density functions (PSD). Replication was carried out in the photopolymer OrmoComp. In Fig. 16 the PSD function for the cross-sectional flycut RSA-501 specimen is exemplarily shown as the functions were similar for each flycut specimen. The PSD function of the flycut workpiece has better surface properties than the embossed and replicated structure. The difference for high spatial frequencies is due to the difference between the flat surface and form of the structure. The differences for mid and lower spatial frequencies indicates that the deformation during the micro-embossing process resulted in an increase of waviness and roughness. For instance, the root mean square heights Sq were calculated from LSM measurements with a measuring field of 50 µm × 50 µm, see Table 3.

The PSD function of the embossed micro-structure and replicated structure are showing very small differences in form for high spatial frequencies. For low spatial frequencies the PSD function of the replicated structure is below the function of the embossed structure. This indicates that the shrinkage of the photopolymer smoothened the surface and resulted in a decrease in roughness.

The effect of the elastic spring back effect can be seen in Fig. 17. The geometry of micro-structures measured by means of AFM was compared to the tool radius. A difference in curvature radius between structure radius R_S = 0.39 mm and tool radius R_r = 0.25 mm can be seen.

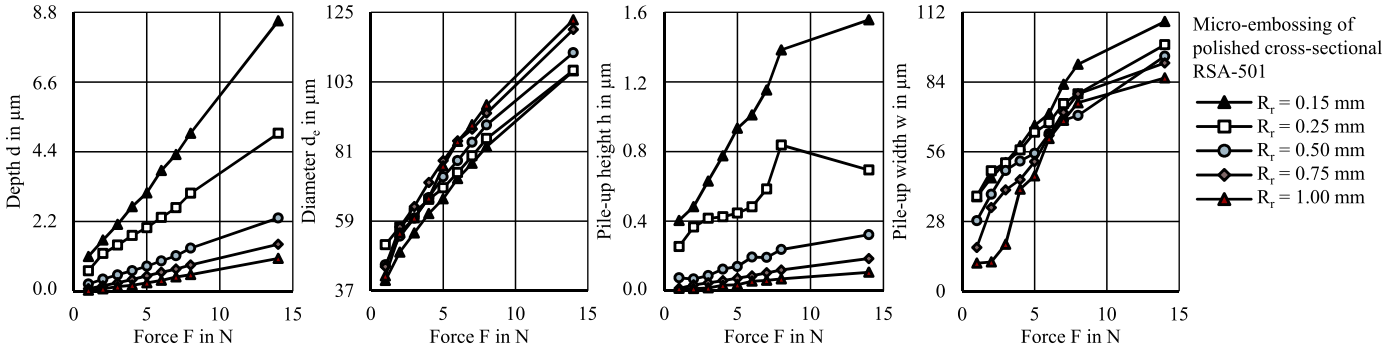

Fig. 14. Micro-embossing of polished cross-sectional RSA-501 with variation of embossing force F and tool radius R_r.

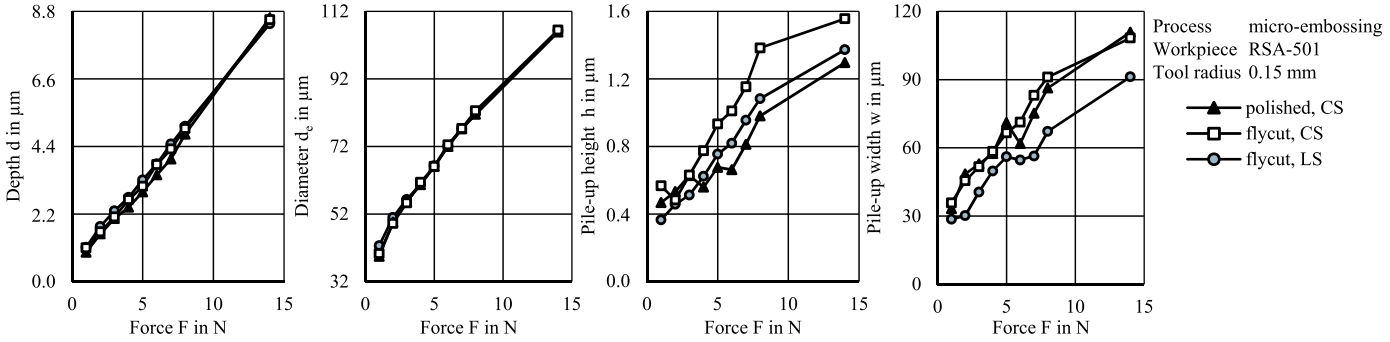

Fig. 15. Micro-embossing of RSA-501 with a spherical ruby tool and variation of the embossing force F.

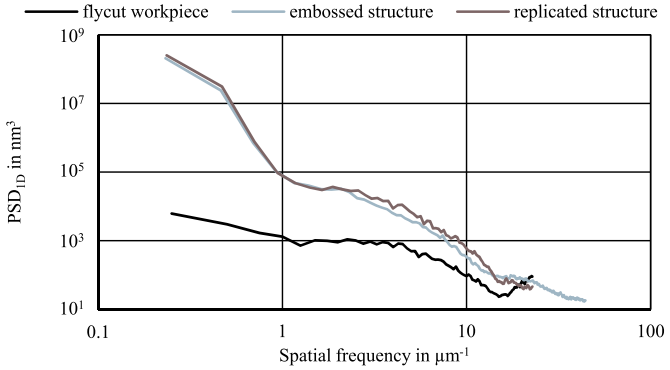

Fig. 16. Power spectral density functions of flycut workpiece, embossed micro-structure and replicated structure.

Table 3
Roughness parameters of workpiece and structures.

Specimen	Root mean square height Sq
Flycut workpiece	6.36 nm
Embossed structure	16.30 nm
Replicated structure	13.58 nm

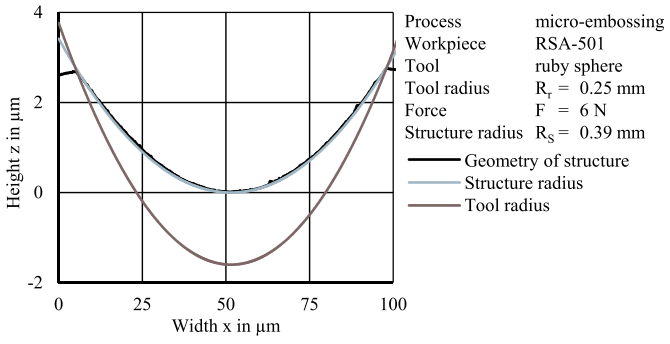

Fig. 17. Difference in curvature radius of embossed micro-structure and tool due to the elastic spring back effect.

5. Discussion

Micrographs of RSA-501 cut in cross and longitudinal sections showed, that grains of RSA-501 were orientated along the extrusion direction due to the rapid solidification process. Grains that are elongated in a direction and not round cause an anisotropy that can influence the cutting and forming process due to the blocking of dislocations through grain boundaries. These processes can be also influenced by the grain sizes since the strength and hardness are affected through the Hall-Petch relation. The difference in the calculated mean grain size of the cross section (d = 0.82 µm) and the longitudinal section (d = 0.90 µm) was small. The reasons for the calculated difference are the elongated grains of the longitudinal section and the caliper method, which uses the maximum length of a grain as its grain size. In fact, the direction of the section influences the shape of grain but not the number of grains, which is the reason why the strength and hardness of both sections should be equal. For micro-embossing the number of grains under the tool is large. Therefore, the material behaves homogeneous. A micro-hardness test confirmed that and resulted in a hardness of 160 HV 0.05 for both sections.

Since the cross section does not have an anisotropic texture, it is recommended to process the cross section. Nonetheless, both sections showed regions of larger grains. There are numerous factors that might cause these regions of larger grains over the long production and preparation processes.

The precipitations and their size in RSA-501 were investigated to figure out if the distribution or size of precipitations could possibly affect the forming of micro-embossments. SEM micrographs in combination with EDX pointed out, that the precipitations in RSA-501 that are likely to be Al_6Mn varied in size. But even Al_6Mn-precipitations of the maximum size of 250 nm do not affect the forming process, since it is known from the literature, that Al_6Mn-precipitations do not affect the hardness [17]. $Al_3Sc_xZr_{1-x}$-precipitations though affect the strength of RSA-501, as literature states [14]. SEM micrographs showed, that the precipitations that are likely to be $Al_3Sc_xZr_{1-x}$ were very fine and homogeneously distributed, so that their effect on the forming of nano-indents or micro-embossments did not depend on the position.

The nanoindentation tests and the investigation of the surface integrity showed that the preparation of the workpiece surface affected the material and its properties. The region of surface integrity was affected by the preparation and a work-hardened surface layer was formed. The nanoindentation process occurred in a thin work-hardened layer, which can be seen in the increase of the E-modulus by 58.3% in relation to the value of the manufacturer. Thus, the strength, E-Modulus and hardness were affected by the surface preparation.

In SEM micrographs of sections of RSA-501 a surface integrity could be observed for flycut but not for polished surfaces. As expected the surface of the polished specimen was not affected by its preparation. On the contrary, the normal forces that occur during flycutting resulted in a surface integrity. However, the depth of the surface integrity s_{max} = 192 nm was not high enough to affect the formation of micro-structures. The difference in the reached indentation depth during nanoindentation and micro-embossing was the reason why the surface integrity affected the nanoindentation process but not the micro-embossing process. Micro-structures embossed with the minimum force of 1 N and a tool with a radius of R_r = 0.15 mm were deeper than 800 nm. On the other hand, nanoindentations in RSA-501 reached a maximum depth h_{max} = 459.8 nm.

Depths d and diameters d_e of micro-embossments in polished and flycut surfaces were of the same size. As shown before, the preparation methods polishing and flycutting affected the surfaces in different ways, but the effect of the surface integrity on the micro-embossing process is neglectable, so that both surface preparation methods had the same result on the formation of micro-structures. The locally varying surface integrity is assumed to have an influence on the standard deviation of the micro-structure geometry values.

Micro-embossments of cross and longitudinal sections had the same geometry values. Hence, the material's texture did not affect the geometry of micro-structures because the texture did not affect the material's hardness. Although the cross section is preferable in terms of grain size and homogeneity, there was no difference between the two sections in terms of structure depth d and diameter d_e for micro-embossing. Therefore, cross and longitudinal sections can be equivalently used for micro-embossing.

The reason for the difference in curvature radius between tool and structure is the elastic spring back during unloading. However, the geometry of the micro-structures stays spherical. Therefore, the structure diameter D_S of embossed concave micro-structures in RSA-501 can be adjusted by choosing the corresponding tool diameter D_r from Fig. 18.

Parametric models were set up from the results of the micro-embossing (see Formulas (5-1) and (5-2)), which make it possible to determine the force F and the tool radius R_r given the structure radius R_S and the structure depth dS. The models allow to determine the process parameters for micro-embossing of convex structures with specific geometries.

$$F = \frac{d_S - 3,19 \bullet {R_r}^4 - 9,35 \bullet {R_r}^3 + 10,46 \bullet {R_r}^2 - 5,44 \bullet R_r + 1,02}{0,09 \bullet {R_r}^{-1,07}} \quad (5\text{-}1)$$

$$R_r = \sqrt{0,34 + \frac{2R_S}{2,84}} - 0,54 \quad (5\text{-}2)$$

6. Conclusion

The production of mold inserts for the replication of MLAs through micro-embossing could be an alternative process route in order to reduce time and costs. The rapidly solidified aluminum alloy RSA-501 is expected to form micro-structures with low surface roughness because of its ultra-fine grain structure. In micro-embossing challenges like elastic spring back effect, pile-ups, and forming accuracy strongly depend on the material's behavior. Therefore, the material RSA-501 was further characterized. Additionally, the influence of the surface preparation on the material's behavior during micro-embossing was investigated.

RSA-501 specimens were cut in cross and longitudinal sections according to the extrusion direction and prepared by either polishing or flycutting. Micrographs of ground, polished and etched specimens showed that the grain structure of RSA-501 was oriented along the extrusion direction. SEM micrographs and EDX mappings were used to analyze the precipitations, their distribution, and size. Al_6Mn-precipitations had a maximum size of 250 nm and were likely located on grain boundaries. The $Al_3Sc_xZr_{1-x}$-precipitations were in the range of nanometers and evenly distributed. EBSD measurements showed that the mean grain sizes of the cross and longitudinal sections were both d < 1 μm. Nanoindentation tests on cross and longitudinal sections and tests on polished and flycut RSA-501 specimens were performed. Polished and flycut RSA-501 specimens were prepared by using a focused ion beam, measured by means of SEM and were analyzed for their depth of surface integrity. The maximum surface integrity depth of flycut specimens was 192 nm while polished specimens were not influenced. Micro-structures were embossed in surfaces prepared by polishing or flycutting and in surfaces of different extrusion directions. The preparation method and extrusion direction had no influence on the geometry of micro-structures.

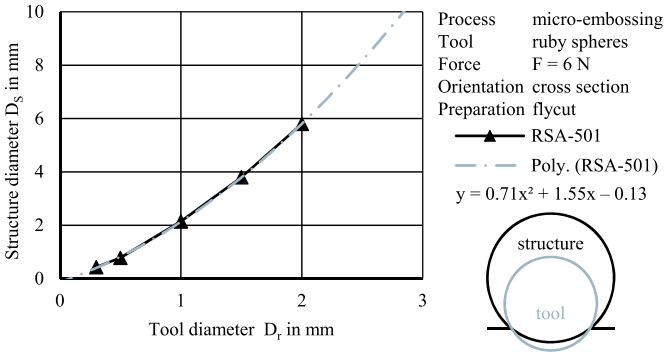

Fig. 18. Correlation between tool diameter D_r and structure diameter D_S.

The induced surface integrity through flycutting was not deep enough to influence the forming of micro-structures. Therefore, the workpiece surface can be prepared either by polishing or flycutting. When micro-embossing RSA-501 cross and longitudinal sections according to the extrusion direction can be used. However, from the material investigations of RSA-501 it is recommended to process the cross section because of its isotropic grain structure.

A difference between tool radius R_r and structure radius R_S was observed due to the elastic spring back effect. However, the structure geometry remained spherical. Therefore, the elastic spring back effect can be compensated by adjusting the tool radius R_r. Furthermore, a parametric model was presented that can be used to calculate the process parameters for micro-embossing of concave structures with specific geometries in RSA-501.

Credit authors statement

Julian Kober Investigation, Writing - Original Draft, Visualization, Project administration, Daniel Rolón Investigation, Writing - Review & Editing, Project administration, Florian Hölzel Investigation, Writing - Review & Editing, Project administration, Stefan Kühne Writing - Review & Editing, Funding acquisition, Expert advicing, Dirk Oberschmidt Writing - Review & Editing, Supervision, Funding acquisition, Thomas Arnold Writing - Review & Editing, Supervision, Funding acquisition.

Declaration of competing interest

The authors declare the following financial interests/personal relationships which may be considered as potential competing interests: Dirk Oberschmidt reports financial support was provided by German Research Foundation.Thomas Arnold reports financial support was provided by German Research Foundation.

Data availability

Data will be made available on request.

Acknowledgements

This work was funded by the Deutsche Forschungsgemeinschaft (DFG, German Reuter Foundation) – 440840282, 452333040, and GZ: INST 131/789-1 FUGG.

References

[1] J.W. Duparré, F.C. Wippermann, Micro-optical artificial compound eyes, Bioinspiration Biomimetics 1 (2006) R1–R16, https://doi.org/10.1088/1748-3182/1/1/r01.

[2] W. Yuan, L.-H. Li, W.-B. Lee, C.-Y. Chan, Fabrication of microlens array and its application: a review, Chin. J. Mech. Eng. 31 (2018) 1–9, https://doi.org/10.1186/s10033-018-0204-y.
[3] M.F. Land, Variations in the structure and design of compound eyes, in: Facets of Vision, Springer, Berlin, Heidelberg, 1989, pp. 90–111.
[4] M. Levoy, P. Hanrahan, Light field rendering, in: Proceedings of the 23rd Annual Conference on Computer Graphics and Interactive Techniques - SIGGRAPH '96, New York, New York, USA, ACM Press, New York, New York, USA, 1996.
[5] S. Scheiding, A.Y. Yi, A. Gebhardt, R. Loose, L. Li, S. Risse, R. Eberhardt, A. Tünnermann, Diamond milling or turning for the fabrication of micro lens arrays: comparing different diamond machining technologies, in: Advanced Fabrication Technologies for Micro/Nano Optics and Photonics IV, 2011, p. 79270N. San Francisco, California, United States, SPIE.
[6] S. Cai, Y. Sun, H. Chu, W. Yang, H. Yu, L. Liu, Microlenses arrays: fabrication, materials, and applications, Microsc. Res. Tech. 84 (2021) 2784–2806, https://doi.org/10.1002/jemt.23818.
[7] S. Kirchberg, L. Chen, L. Xie, G. Ziegmann, B. Jiang, K. Rickens, O. Riemer, Replication of precise polymeric microlens arrays combining ultra-precision diamond ball-end milling and micro injection molding, Microsyst. Technol. 18 (2012) 459–465, https://doi.org/10.1007/s00542-011-1414-8.
[8] S. Scheiding, A.Y. Yi, A. Gebhardt, L. Li, S. Risse, R. Eberhardt, A. Tünnermann, Freeform manufacturing of a microoptical lens array on a steep curved substrate by use of a voice coil fast tool servo, Opt Express 19 (2011) 23938–23951, https://doi.org/10.1117/12.874751.
[9] D.A. Rolón, M. Jagodzinski, S. Kühne, S. Gebauer, M. Malcher, D. Oberschmidt, Technological investigation for production of metallic micro-optics employing embossing process, in: 20th International Conference Proceedings, euspen, Cranefield, Geneva, 2020.
[10] DIN Deutsches Institut für Normung e.V, Fertigungsverfahren Druckumformen: Teil 5: Eindrücken, Beuth, Berlin, 2003.
[11] X. Chang, K. Xu, D. Xie, S. Luo, X. Shu, H. Ding, K. Zheng, B. Li, Microforging technique for fabrication of spherical lens array mold, Int. J. Adv. Manuf. Technol. 96 (2018) 3843–3850, https://doi.org/10.1007/s00170-018-1719-1.
[12] R. ter Horst, M. de Haan, G. Gubbels, R. Senden, B. van Venrooy, A. Hoogstrate, Diamond turning and polishing tests on new RSP aluminum alloys, in: Modern Technologies in Space- and Ground-Based Telescopes and Instrumentation II, SPIE, Amsterdam, Netherlands, 2012, p. 84502M.
[13] S. Grabarnik, M. Taccola, L. Maresi, L. de Vos, V. Moreau, J. Versluys, G. Gubbels, Compact multispectral and hyperspectral imagers based on a wide field of view TMA, in: International Conference on Space Optics — ICSO 2010, Rhodes Island, Greece, 2010. SPIE.
[14] F. Palm, Scalmalloy - A Unique High Strength and Corrosion Insensitive AlMgScZr Material Concept, 2008. Aachen.
[15] J. Murray, A. Peruzzi, J.P. Abriata, The AI-Zr (Aluminum-Zirconium) system, J. Phase Equil. 13 (1992), https://doi.org/10.1002/0471740039.vec0942.
[16] P. Bajaj, Precipitation during Intrinsic Heat Treatment in Laser Additive Manufacturing, Dissertation, Aachen, 2020.
[17] M. Vlach, I. Stulikova, B. Smola, T. Kekule, H. Kudrnova, S. Danis, R. Gemma, V. Ocenasek, J. Malek, D. Tanprayoon, V. Neubert, Precipitation in cold-rolled Al–Sc–Zr and Al–Mn–Sc–Zr alloys prepared by powder metallurgy, Mater. Char. 86 (2013) 59–68, https://doi.org/10.1016/j.matchar.2013.09.010.
[18] M. Geiger, M. Kleiner, R. Eckstein, N. Tiesler, U. Engel, Microforming, CIRP Annals 50 (2001) 445–462, https://doi.org/10.1016/S0007-8506(07)62991-6.
[19] U. Engel, R. Eckstein, Microforming—from basic research to its realization, J. Mater. Process. Technol. 125–126 (2002) 35–44, https://doi.org/10.1016/s0924-0136(02)00415-6.
[20] A. Rosochowski, W. Presz, L. Olejnik, M. Richert, Micro-extrusion of ultra-fine grained aluminium, Int. J. Adv. Manuf. Technol. 33 (2007) 137–146, https://doi.org/10.1007/s00170-007-0955-6.
[21] H. Justinger, Experimentelle und numerische Untersuchung von Miniaturisierungseinflüssen bei Umformprozessen am Beispiel Mikro-Tiefziehen, Diss., Shaker, Aachen, 2009.
[22] W.C. Oliver, G.M. Pharr, An improved technique for determining hardness and elastic modulus using load and displacement sensing indentation experiments, J. Mater. Res. 7 (1992) 1564–1583, https://doi.org/10.1557/jmr.1992.1564.
[23] Rsp Technology, RS Alloys Overview, 2018. https://www.rsp-technology.com/site-media/user-uploads/rsp_alloys_overview_2018lr.pdf. (Accessed 4 January 2022). accessed.
[24] J.P. Davim, Surface Integrity in Machining, Springer London, London, 2010.